Draft version May 3, 2016
Preprint typeset using LaTeX style emulateapj v. 01/23/15

OBSERVATIONS OF THE TYPE IIN SN J13522411

Ryan Hofmann and Nathan Smith
Steward Observatory, University of Arizona
Draft version May 3, 2016

ABSTRACT

We present visible and near-IR photometry and spectra of the type IIn supernova PSN J13522411. The light curve indicates a peak < 50 days after discovery around $M = -17$, followed by a slow decline. Spectra show strong hydrogen and helium emission that peaks ~ 200 d after discovery, with a P-Cygni profile that becomes more absorptive as time progresses. We determine that the CSM is in the form of a slow, dense stellar wind that has remained steady for 30 years. The low velocity of the wind, ≈ 70 km/s, implies that the progenitor was probably a red or yellow supergiant. From the light curve, we estimate the total radiated energy to be $\sim 10^{50}$ erg. Further details of the explosion will be determined as time allows.

1. INTRODUCTION

Understanding the explosive deaths of massive stars as supernovae is an important area of astrophysical research, as it is through this process that heavy elements are formed and dispersed into the interstellar medium. The expanding shocks from supernovae are also a key player in initiating and ending local star formation, as well as driving galactic winds. One of the more interesting aspects of these phenomena, and one that is still not well understood, is how supernovae interact with their environments. A striking example of this interaction is the class SNe IIn, which have narrow emission lines and slowly declining light curves (Filippenko 1997).

Most of the peculiar features of SNe IIn can be explained by a shell of dense circumstellar material ejected from the star before it exploded. Initially after the star explodes, intense UV- and X-ray radiation from the hot forward shock photoionize the slow-moving CSM, producing narrow-line emission with a Lorentzian profile. Later, the rapidly expanding shock collides with the CSM, causing broad emission with a line profile that depends on the distribution of the CSM.

There are two main ways that a star may develop a dense CSM before it explodes. The first, and arguably simplest, origin is a dense stellar wind, which is usually driven by very high luminosity, as in Wolf-Rayet stars, and/or by high opacity in the outer layers of the star, as would be expected in a red supergiant. In the case of Wolf-Rayet stars, this wind typically blows at hundreds or even thousands of kilometers per hour, effectively peeling away the star's outer layers; if the density of the stellar wind is relatively low, these stars will explode as type Ib or Ic SNe. Whereas in the case of red supergiants, the stellar wind may only blow at 100 km/s or less, but the density can be much greater; these stars, without a dense CSM, would typically explode as type IIL or IIP SNe.

The second method of producing a dense CSM is in bursts, typically eruptions driven by the complex internal dynamics of the star as it burns heavier elements. One of the best known instances of a star undergoing such eruptions would be the luminous blue variable (LBV) Eta Carinae, which erupted in 1841 and briefly became the second-brightest star in the sky. Today, we see the remnants of that eruption as a huge bipolar nebula called the Homunculus.

There is a third mechanism for creating a substantial CSM, and that is by shedding angular momentum, either from a rapidly rotating single star or from the merger of a binary. One well-known example of this is SN 1987A, the progenitor of which was determined to be a blue supergiant. More than ten years after the explosion, the shock wave began colliding with a dense ring of material which was shed $\sim 20,000$ years ago (Fransson et al. 2015). As the expanding shock moves through and interacts with the ring and the surrounding CSM, it will reveal details of the mass loss history of the progenitor that will hopefully help to determine whether the ring originated in the single or binary model. It is unknown whether such structures are common for massive stars, as 1987A is one of only a handful of SNe to be continuously monitored for many years after the explosion; most SNe are in distant galaxies, and thus become too faint to observe in this manner. Had 1987A exploded in a distant galaxy, we might never have known about the ring of CSM and its implications. Likewise, if it had exploded just a few years after the ring was produced, 1987A might have been classified as a type IIn SN. For this and other reasons, SNe IIn are a complex and varied class of objects with a wide range of histories, and every instance is unique and worth careful analysis.

In this paper, we present visual and near-IR photometry and spectroscopy of PSN J13522411 from discovery up to ~ 450 d afterward. PSN J13522411 was discovered by Zhangwei Jin and Xing Gao on 2015 Jan. 14.9 in three unfiltered images of NGC 5337. The reported apparent magnitude was 16.9, which we assume to be equivalent to the R magnitude, but is more likely to be an upper limit. No source was visible in images taken on Jan. 07 (limiting mag 19.5). It was classified as having a type IIn spectrum on 2015 Jan. 16.9 by Jujia Zhang and Xiaofeng Wang. At a redshift of $z = 0.007007$ (2165 km/s), this corresponds to a distance of 36.39 Mpc ($m - M = 32.8$ mag), with a Milky Way line-of-sight extinction $A_v = 0.038$ mag and reddening $E(B-V) = 0.013$ mag. PSN J13522411 resides in the outer disk of NGC 5337, at a projected separation of ~ 18 arcsec (~ 3 kpc) from the host galaxy's nucleus.

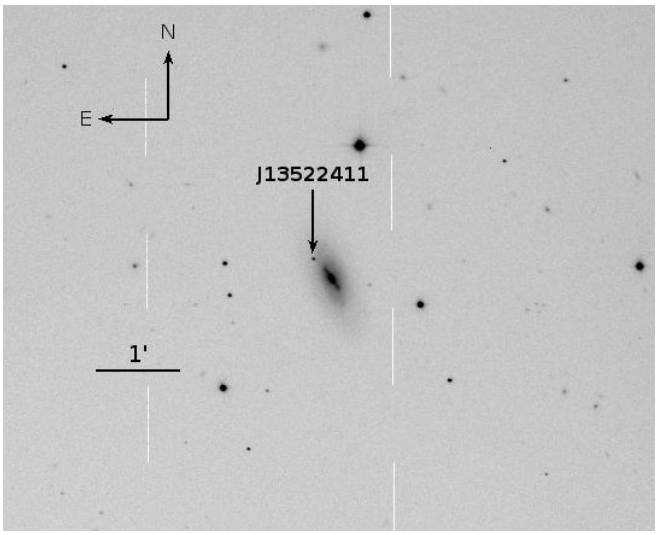

Figure 1. R-band image of NGC 5337 taken on 2016 March 17 with the Kuiper 61-inch telescope. PSN J13522411 is indicated by the arrow. The repeating vertical lines are bad columns.

Our observations are presented in Section 2, and the light curve and spectral evolution are analysed in Section 3. Section 4 provides a summary of our work.

2. OBSERVATIONS

2.1. *Discovery*

PSN J13522 was discovered on three 40-s survey images taken with an unfiltered CCD on a Celestron C14 Schmidt-Cassegrain telescope (Jin and Gao 2015). The object first appeared on 2015 Jan. 09.9, and was confirmed on 2015 Jan. 14.9; nothing was visible in images taken on 2015 Jan. 07 (limiting mag 19.5). The object was spectroscopically classified as a type IIn on 2015 Jan. 16.9 (Zhang and Wang 2015).

2.2. *SLOTIS photometry*

After discovery of PSN J13522, the field was added to the queue of the robotic Super-LOTIS 24-inch telescope (SLOTIS; Williams et al. 2008) on Kitt Peak for multifilter (B, V, R, and I) follow-up observations. Seeing varied between $\sim 2-4$ arcsec. Images were automatically calibrated using a custom pipeline by Peter Milne, and aperture photometry was performed manually. The magnitudes were calibrated using the reference star list from the SLOTIS pipeline, shown in Table 4. The photometry is summarized in Table 1.

2.3. *UKIRT JHK photometry*

Three sets of JHK images were collected during the same period as the SLOTIS data, using the UK Infrared Telescope's (UKIRT) Wide Field Camera instrument (WFCAM; Hodgkin et al. 2009). The 'seeing', estimated from the full width at half-maximum intensity (FWHM) of stars on the CCD frame, varied between $\sim 1-2$ arcsec. Aperture photometry was performed manually, and the magnitudes were calibrated using the same reference stars from SLOTIS. The results are summarized in Table 2.

2.4. *Kuiper BVR photometry*

Table 1
SLOTIS photometry

Time (days)	Filter	Mag (mag)	σ (mag)	Filter	Mag (mag)	σ (mag)
111	B	17.273	0.216	V	16.692	0.068
111	R	15.97	0.032	I	15.173	0.029
113	B	17.603	0.131	V	16.535	0.061
113	R	16.06	0.034	I	15.131	0.034
115	B	17.201	0.083	V	16.785	0.049
115	R	15.906	0.021	I	15.1	0.024
125	B	16.974	0.052	V	16.695	0.048
125	R	16.031	0.03	I	15.216	0.027
131	B	17.439	0.13	V	16.915	0.056
131	R	16.073	0.029	I	15.196	0.025
134	B	17.342	0.261	V	16.869	0.071
134	R	16.194	0.045	I	15.289	0.032
137	B	17.005	0.078	V	16.971	0.096
137	R	16.163	0.038	I	15.323	0.037
140	B	17.223	0.128	V	17.017	0.074
140	R	16.278	0.047	I	15.429	0.046
155	B	-	-	V	16.924	0.045
155	R	16.141	0.022	I	-	-
158	B	-	-	V	16.816	0.045
158	R	16.14	0.024	I	-	-
349	B	-	-	V	-	-
349	R	16.894	0.027	I	16.257	0.055
363	B	-	-	V	17.527	0.036
363	R	16.869	0.039	I	-	-
404	B	18.149	0.109	V	17.948	0.077
404	R	17.085	0.079	I	16.754	0.083

Table 2
UKIRT photometry

Time (days)	J (mag)	σ_J (mag)	H (mag)	σ_H (mag)	K (mag)	σ_K (mag)
108	14.074	0.009	13.631	0.01	13.27	0.015
142	14.409	0.009	13.942	0.011	13.455	0.015
157	14.521	0.009	14.061	0.011	13.547	0.015

Table 3
Kuiper photometry, day 428

Filter	mag	σ (mag)
B	18.437	0.083
V	18.020	0.063
R	17.112	0.035

One set of images was recorded at a late time using the Mont4k CCD on the 61" Kuiper telescope on Mt. Bigelow (Fontaine et al. 2014). Seeing was < 0.5 arcsec. The R-band image with compass and scale is shown in Figure 1. Aperture photometry was performed manually. Some of the reference stars were outside the field of view or saturated, and were thus excluded from the reduction. The results are summarized in Table 3.

2.5. *Spectroscopy*

Five high-resolution spectra were obtained using the Bluechannel (BC) spectrometer on the MMT with the 1200 line grating. Four of the spectra were taken during

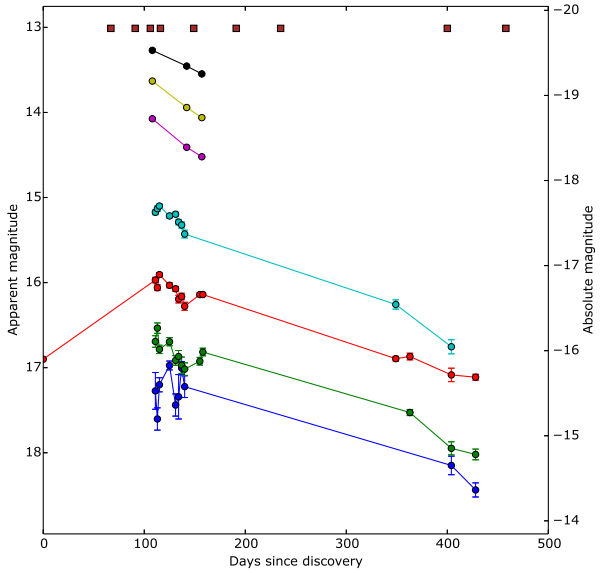

Figure 2. Photometric data for PSN J13522411. SLOTIS data in B, V, R, and I are plotted around 100-160 days in blue, green, red, and cyan, respectively. The discovery magnitude is plotted in red at far left, and the Kuiper data are plotted at the far right. UKIRT data in J, H, and K are plotted in magenta, yellow, and black, respectively. Dates for which spectral data are available are marked in brown at the top. All magnitudes have been corrected for Milky Way reddening.

Table 4
Spectral observations of PSN J13522411

Time (days)	Obs./Instr.	Range (Å)
67	MMT/BlueChan	5700-7000
91	LBT/MODS	6500-8600
106	MMT/BlueChan	5700-7000
116	MMT/BlueChan	5700-7000
149	MMT/BlueChan	5700-7000
191	Shane/Kast	3400-10800
235	Shane/Kast	3400-10800
400	MMT/BlueChan	5700-7000
458	Bok/B&C	4000-8300

the first six months, while the fifth was taken much later. One early spectrum was obtained using the Multi Object Double Spectrograph (Byard and O'Brien 2000, MODS) on the LBT. Two broad spectra were obtained using the Kast spectrograph on the Lick 3-m Shane reflector (Miller and Stone 1993). Finally, one late-time spectrum was obtained using the Boller & Chivens (B&C) spectrograph on the Bok 90-inch telescope on Kitt Peak. All spectra were Doppler-corrected, and the broad spectra were also corrected for reddening. The full spectra are plotted in Figure 3, and details of the spectra are summarized in Table 4.

3. ANALYSIS

3.1. *Light curve*

3.1.1. *General features*

The multiband light curves of PSN J13522411 are shown in Figure 2. No data is available around the time of peak luminosity, so the exact peak date could be anywhere between $\sim 10-50$ days. Likewise, the later portion of the light curve has a > 250 d gap where no data was taken, so we can only assume that the decline during this period is basically linear. Despite the lack of sampling, it is clear that the SN is decaying quite slowly: in ~ 300 days, the R brightness only decreased by ~ 1.1 mag. This is much slower than would be expected from just the decay of radioactive cobalt, indicative of the strong interaction between the expanding shock and the CSM. For how long-lived it is, however, the SN is unusually dim. This may be due to extinction effects, either from the remaining cold CSM or from the host galaxy. In §3.2.5, we use the sodium doublet to estimate reddening due to the host galaxy, concluding that $E(B-V)_{host} \approx 0.39$ mag. Assuming a similar reddening law to the Milky Way, this implies an additional $A_{R,host} = 0.585$ mag. We have not applied this correction to the light curve.

3.1.2. *Total emitted energy*

If we assume that the R-band brightness is roughly equivalent to the bolometric magnitude, we can transform the R magnitudes into luminosities and integrate over time to get an estimate of the total radiated energy. Performing this calculation (Aretxaga et al. 1999), we estimate the total emitted energy to be $\sim 4 \times 10^{49}$ erg. Because we were not able to obtain any data during the period around maximum brightness, this value is probably a lower limit, putting the true value closer to $\sim 10^{50}$ erg. In fact, using the correction factor we calculated in §3.1.1, our lower bound increases to $\sim 7 \times 10^{49}$ erg, a more reasonable value for a SN IIn.

3.2. *Spectral evolution*

3.2.1. *General properties*

Besides the H-alpha line discussed below, the spectra from Lick Observatory also show H-beta emission (weakly visible in Bok), bright emission lines from calcium in the near-infrared around ~ 8500 angstroms, and other broad emission lines. The line at 5876 angstroms is bisected by strong absorption from the sodium D doublet. The H-alpha line also features several small absorption lines between $\sim 6450 - 6525$ angstroms.

3.2.2. *Continuum*

Initially, the continuum of PSN J13522411 was flat over the range of the MMT, while the LBT spectrum showed emission and absorption features in the near-infrared. Over the next few months, the continuum became more red, as seen in both the MMT and Lick spectra. This trend reversed sometime around 400 days after discovery, as the last MMT spectrum seems less diagonal, while the final spectrum from Bok has a blue continuum with a clear peak around ~ 5000 angstroms, implying an effective temperature of ~ 5800 K.

3.2.3. *H-alpha line evolution*

Refer to Figure 4. Initially, the broad H-alpha line is symmetrical with a FWHM of ~ 1400 km/s, with Lorentzian wings extending out to $\sim \pm 5000$ km/s. On

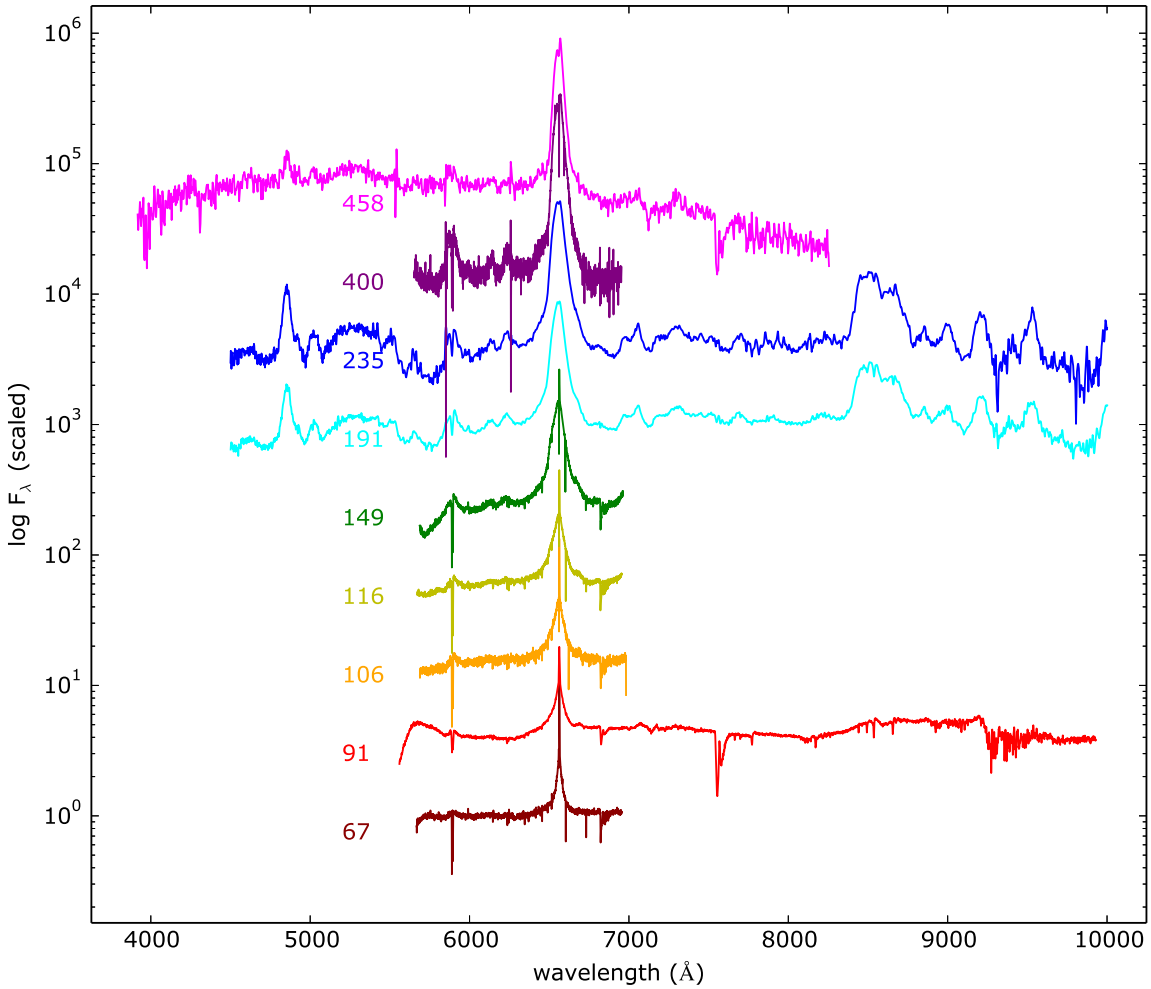

Figure 3. All spectra of PSN J13522411, with early times at the bottom and later times at the top. The spectra have been normalized to the continuum at 6300 angstroms.

top of the broad component is a narrow P-Cygni feature, predominately emission, with a Gaussian FWHM of $\sim$ 50 km/s, about the resolution of the grating. As time progresses, the broad emission increases and becomes more humped until $\sim$ 200 d after discovery, after which the H-alpha flux starts to decrease; the overall profile, however, remains roughly symmetrical, indicating a relatively even distribution of CSM. The P-Cygni feature gradually transitions from mostly emission to almost all absorption, causing the appearance of a double peak in the broad emission; this indicates that there is still a great amount of cold gas surrounding the star that has not yet been illuminated. The FWHM of the broad emission rises rapidly, peaks around $\sim$ 200 d after discovery, then declines more gradually. At late times, very low, broad wings develop that extend out to $\sim$ 8000 km/s; these wings are an indication that the photosphere has receded, revealing the extremely high-velocity material behind the reverse shock. The peak-to-trough width of the P-Cygni feature remains roughly constant at $\sim$ 70 km/s, indicating a stellar wind that has not varied much over time.

3.2.4. *CSM properties*

Taking half the FWHM as the velocity of the shock, we estimate the radius of the CSM with the following relation: $R_{CSM} \geq \frac{1}{2} \times v_{shock} \times \Delta t$. Plugging in $v_{shock} = 3500$ km/s and $\Delta t = 458d$ (see Figure 5), we determine the radius to be $\sim 460AU$. If we assume that the peak-to-trough width of the P-Cygni feature indicates the velocity of the CSM, $v_{CSM} \approx 70$ km/s, we arrive at a lower age limit of $\sim$ 31 years; this may imply that the progenitor underwent little change in luminosity and was comparatively stable during the later stages of nuclear burning. The low velocity of the CSM, likely a smooth stellar wind, indicates that the progenitor was most likely a red or yellow supergiant (Smith et al. 2015), rather than a Wolf-Rayet star or LBV. That the H-alpha emission remains as bright as it does at such late times and large distances suggests that the stellar wind was rela-

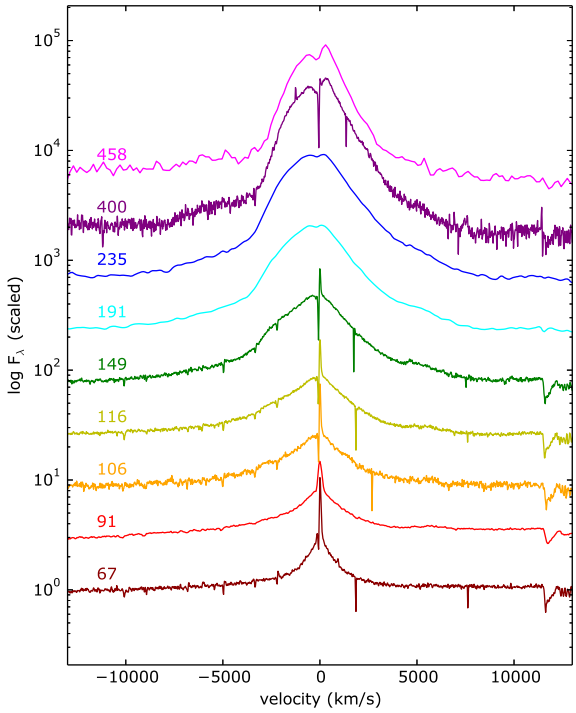

Figure 4. Evolution of the H-alpha profile, normalized to the continuum at 6300 angstroms (12263 km/s). The sharp dips at ∼2000 km/s are bad pixels. The absorption features at the far right are telluric lines.

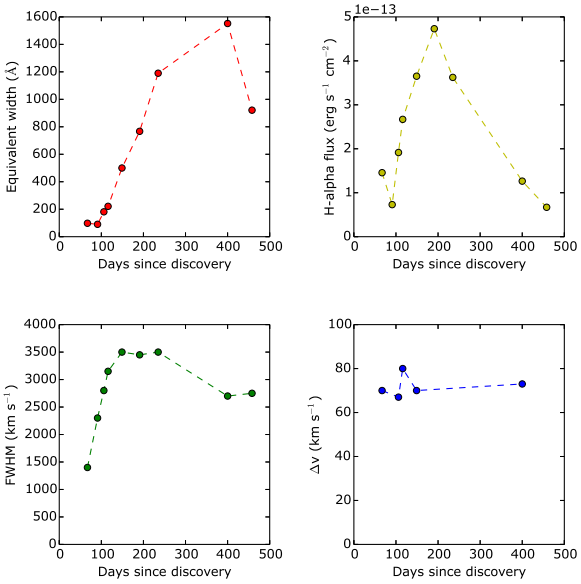

Figure 5. Properties of the H-alpha line, plotted over time. Top left: Equivalent width, measured between 6300-6800 angstroms. Top right: total flux of H-alpha emission, from the equivalent width measurements. Bottom left: FWHM of the broad H-alpha line. Bottom right: Peak-to-trough width of the P-Cygni profile in the high-resolution spectra.

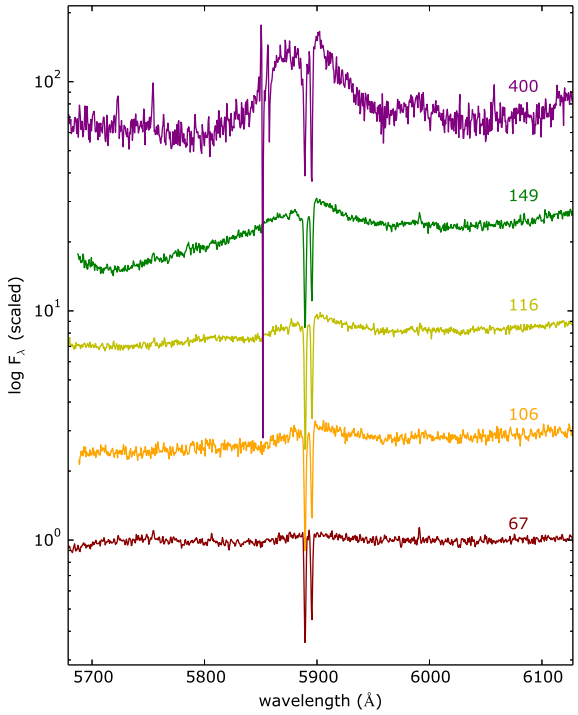

Figure 6. Sodium emission with strong doublet absorption. The sharp spike at left in the top spectrum is likely a bad pixel.

tively dense; the exact density and mass-loss rate will be determined at a later time.

3.2.5. *Host reddening*

Using the Na D doublet, shown in close-up in Figure 6, we can estimate the amount of reddening due to dust in the host galaxy (Poznanski et al. 2012). Measuring the equivalent width of each line and comparing to the respective chart of equivalent width vs. reddening, we estimate $E(B-V)_{host} \approx 0.39$ mag. We have not applied this correction to either the light curve or the spectra, but we discuss the implications for the total energy in §3.1.2. This reddening would also affect our determination of the peak wavelength and effective temperature of the Bok spectrum (see §3.2.2).

4. CONCLUSION

We obtained photometry and spectra of PSN J13522411 covering the early and later portions of the SN's decline. By integrating the light curve, we estimate the total radiated energy at $\sim 10^{50}$ erg. From the spectral data, we infer that the CSM is a dense, roughly symmetrical stellar wind that had been blowing for at least the last 30 years before the explosion. We also infer from the velocity of the stellar wind that the progenitor was likely a red or yellow supergiant with no obvious signs of severe pre-SN instability. Due to time constraints, we have not yet completed our analysis of this SN. In the coming weeks, we plan to determine the mass and distribution of the CSM, the mass-loss rate due to the stellar wind, and the total energy of the explosion.

5. ACKNOWLEDGEMENTS

Special thanks goes to Dr. Jennifer Andrews for her assistance with data management and reduction; to the faculty and students of Steward Observatory who helped to produce the Kuiper data; and to Dr. Peter Milne, Principal Investigator for the Super-LOTIS robotic telescope, for his assistance in reducing Super-LOTIS data.

REFERENCES

Aretxaga I. et al., 1999, MNRAS, 309, 343
Byard P. L., O'Brien T. P., 2000, Proc. SPIE, 4008, 934
Filippenko A. V., 1997, ARA&A, 35, 309
Fontaine G. et al., 2014, ASP Conference Series, 481, 19
Fransson, C. et al., 2015, The Astrophysical Journal Letters, 806, L19
Hodgkin S. T. et al., 2009, MNRAS 394, 675
Jin Z., Gao X., 2015, CBAT "Transient Object Followup Reports", PSN J13522411+3941286
Miller J. S., Stone R. P. S., 1993, Lick Obs. Tech. Rep. 66, Lick Obs., Santa Cruz
Poznanski D. et al., 2012, MNRAS, 426, 1465
Smith N. et al., 2015, MNRAS, 449, 1876
Williams G. G. et al., 2008, AIP Conference Proceedings, 1000, 535
Zhang J., Wang X., 2015, ATel, 6939